COMMUNICATION

Molecular Dopant Determines the Structure of a Physisorbed Self-Assembled Molecular Network

Received 00th January 20xx,
Accepted 00th January 20xx

DOI: 10.1039/x0xx00000x

Roelof Steeno,[a] Andrea Minoia,[b] Maria C. Gimenez-Lopez,[c#] Matthew Blunt,[d] Neil R. Champness,[c] Roberto Lazzaroni,[b] Kunal S. Mali,*[a] and Steven De Feyter*[a]

A small percentage of an impurity present in the solid state was shown, via scanning tunneling microscopy, to drastically change the on-surface self-assembly behavior of an aromatic tetracarboxylic acid, by initiating the nucleation and growth of a different polymorph. Molecular modelling simulations were used to shed further light onto the dopant-controlled assembly behaviour.

Molecular impurities can have a strong influence on the outcome of crystallization processes. If impurities are added on purpose, then they are referred to as additives. Modern methods of polymorph screening often employ tailor-made additives to control the size and/or the shape of the final crystal and sometimes the polymorphic form itself. Despite its widespread use, the mechanism of action for such additives at the molecular level is not completely understood.[1]

Physisorbed self-assembled monolayers of organic molecules provide an interesting testbed for understanding the influence of additives on crystallization processes occurring under reduced dimensionality. The so-called 2D crystallization of organic molecules has been studied intensively using scanning tunneling microscopy (STM).[2-4] Despite the lack of chemical sensitivity, sub-molecular resolution STM imaging has often proven to be useful for understanding the influence of different additives on molecular self-assembly.[5-8]

Molecular additives have been used with different objectives in the context of self-assembly on surfaces. The two prominent cases involve chiral induction experiments[9] and host-guest chemistry.[10] In the popular sergeant-soldiers approach, a small percentage of structurally similar chiral molecule (*the sergeant*) is used to bestow a defined handedness to the network formed by achiral molecules (*the soldiers*) to produce a homochiral surface.[11] The chiral inducers typically affect the handedness of the network without changing the unit cell. In host-guest chemistry, the additive is a guest molecule that either adsorbs into to host cavities or dynamically changes an otherwise dense network into a porous one *via* templating effect.[12, 13] Additives have also been used for the selection of a specific 2D polymorph,[14] and for initiating bilayer growth.[15]

Here, we describe the self-assembly of *p*-terphenyl-3,3”,5’,5”-tetracarboxylic acid (**TPTC**, Fig. 1a) at the nonanoic acid/graphite interface. STM data revealed that **TPTC** assembles into an unusual network in which the molecules form parallel, hydrogen-bonded arrays together with the anticipated random tiling network reported earlier.[16, 17] Further scrutiny revealed that the parallel network is formed due to the presence of a small amount of a structurally similar impurity, *p*-quaterphenyl-3,3”’,5,5”’-tetracarboxylic acid (**QPTC**, Fig. 1b) present in the solid state. We investigated the additive-controlled dynamic 2D crystallization behaviour with a combination of STM measurements and molecular modelling simulations. Furthermore, a characteristic polymorph-selective bilayer formation behavior is also described.

The self-assembly of **TPTC** at the nonanoic acid/graphite interface, where it forms a random tiling network such as the one displayed in Fig. 1e, has been reported previously.[16, 17] The random tiling network is formed as a result of two degenerate hydrogen bonding modes (Fig. 1c) which arise due to the near equal distance between the phenyl rings of two **TPTC** molecules that are involved in intermolecular hydrogen bonding (d_1) and the distance between the outermost phenyl rings within a **TPTC** molecule (d_2) . In the parallel motif, the hydrogen bonded arrays are formed in a way that the long axis of the terphenyl backbones remains parallel to each other whereas in the arrowhead motif depicted in Fig. 1c, the molecules are oriented 60° with respect to each other. A structurally similar quaterphenyl derivative (**QPTC**, Fig. 1b) assembles exclusively using the parallel hydrogen bonding motif. Since $d_2 > d_1$, **QPTC** cannot form a random tiling network in which all H-bonding valences are satisfied (*vide infra*) unless templated by guest molecules and thus forms an ordered parallel array of molecules as displayed in Fig. 1f.[13] Note that the STM images presented in Fig. 1e and 1f were obtained using the **TPTC** and **QPTC** derivatives synthesized and purified in-house (see ESI).

Fig. 2a shows an STM image of the **TPTC** monolayer formed at the nonanoic acid/graphite interface. In this case, a

[a.] *Division of Molecular Imaging and Photonics, Department of Chemistry, KU Leuven, Celestijnenlaan 200F, B-3001 Leuven, Belgium. Email: kunal.mali@kuleuven.be, steven.defeyter@kuleuven.be*
[b.] *Laboratory for Chemistry of Novel Materials, Materials Research Institute, University of Mons, Place du Parc 20, 7000 Mons, Belgium*
[c.] *School of Chemistry, University of Nottingham, Nottingham, NG7 2RD, UK. #Present address: Centro Singular de Investigacion en Quimica Biolóxica e Materiais Moleculares (CiQUS), Universidade de Santiago de Compostela, 15782 Santiago de Compostela, Spain*
[d.] *Department of Chemistry, University College London, 20 Gordon Street, London, WC1H 0AJ, UK.*
† Footnotes relating to the title and/or authors should appear here.
Electronic Supplementary Information (ESI) available: [details of any supplementary information available should be included here]. See DOI: 10.1039/x0xx00000x

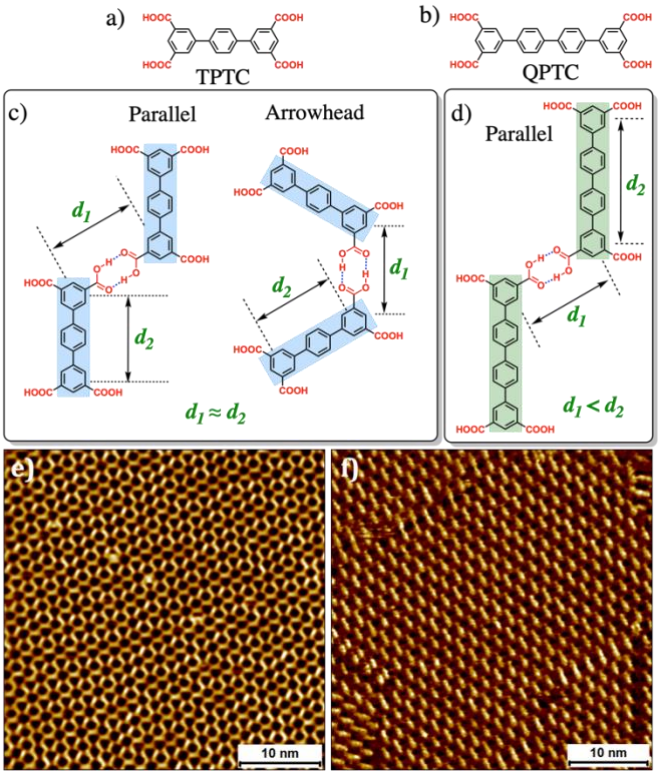

Fig. 1. (a, b) Molecular structures of **TPTC** and **QPTC**, respectively. (c) Schematic showing the parallel and arrowhead H-bonded motifs formed by **TPTC**. As a result of the similarity between d_1 and d_2, **TPTC** forms parallel as well as arrowhead motifs whereas **QPTC** can only form the parallel H-bonded motif as depicted in panel (d). (e, f) STM images showing the random tiling network formed by **TPTC** and the parallel network formed by **QPTC**, respectively at the nonanoic acid/HOPG interface.

commercially procured sample of **TPTC** (Sigma-Aldrich, 99.9%) was used without further purification. The self-assembly of commercial **TPTC** leads to the formation of the parallel network together with the anticipated random tiling network (Fig. S1 in the ESI). Careful examination of the STM data revealed that the domains of the parallel phase were comprised of molecules with different lengths. Features with three different lengths (~2.5 nm, ~1.9 nm and ~1.5 nm) could be identified from the STM data and only the shortest features were found to match approximately with the expected length of the **TPTC** molecule (Fig. 2a, b). This observation is rather surprising given the stated high purity of the **TPTC** sample. Based on the sizes of the observed features, we attribute the longer features to the corresponding *p*-quaterphenyl (**QPTC**, green Fig. 2b) and *p*-quinquephenyl (**QQPTC**, red Fig. 2b) (Fig. S2 in the ESI) tetracarboxylic acids present as an impurity in the solid state. NMR data revealed that the percentage of QPTC in the commercial sample was ~2.5% (see NMR data in the ESI).

Analysis of the STM data revealed that the overall surface area occupied by **QPTC** in the monolayer is ~40% whereas the percentage of **QPTC** present in the domains of the parallel phase alone is ~50%. The overall surface coverage of **QQPTC** is rather small (~5%). Molecular modelling simulations revealed that the adsorption energy of **QPTC** on graphite (-63.7 kcal mol^{-1}) is higher than that of **TPTC** (-52.0 kcal mol^{-1}), given the larger size of the former (computational details provided in the ESI). The higher adsorption energy of **QPTC** means that it nucleates preferentially on the graphite surface and contributes to the mixed monolayer. Molecular models also reveal that due to $d_2 > d_1$ (Fig. 1d), **QPTC** cannot form an extended random tiling network similar to that formed by **TPTC** (ESI Fig. S3). Simulations confirm that **TPTC** on the other hand, can form parallel as well as arrowhead H-bonding motif (ESI Fig. S4). We hypothesize that the nucleation of **QPTC** forces **TPTC** to assemble using the parallel H-bonding motif as it is the preferred motif for **QPTC**. This behavior is reminiscent of the *sergeant-soldiers* experiment except that the percentage of surface-adsorbed *sergeants* is often far lower than the coverage of **QPTC** observed here.

The parallel phase, which is made up of co-adsorbed **QPTC** and **TPTC** molecules (Fig. 3a, b), was found to undergo a slow transition to the random phase. Fig. 3c shows the change in the surface coverage of the parallel phase with time. Initially, the surface is composed of approximately equal percentage of the parallel and the random phase. A noticeable decrease in the number and the size of domains of the parallel phase was observed after about 6 to 7 hours. The **QPTC** impurities are also present in the random phase, but they are found mostly along the domain borders. The surface coverage of the parallel phase reduced significantly after an additional 1 to 2 hours (Fig. S5 in the ESI). The gradual change in the surface coverage of the two networks indicates that the initially observed parallel phase is a kinetic structure that evolves into the thermodynamically favoured random phase. Since the estimation of the surface coverage of monolayer phases is often prone to large errors, the coverage of individual **TPTC** and **QPTC** molecules was measured by analysing the high-resolution STM data.

Quite interestingly, the phase transition described above was found to be associated with a distinct change in the composition of the monolayer. The surface coverage of **QPTC** molecules decreased as a function of time. The time-dependent changes in the composition of the monolayer are summarized in Figure 3d. Within five hours after deposition, there is only a

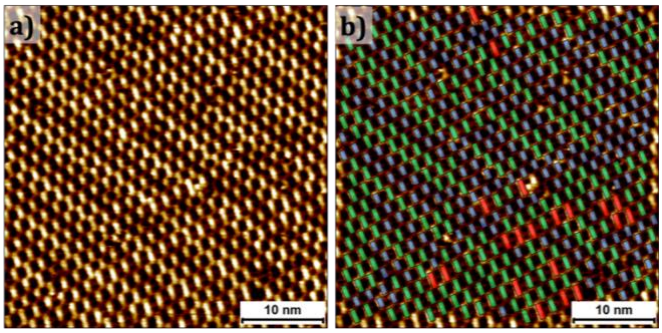

Fig. 2. (a) STM image of the self-assembled network formed by commercially obtained **TPTC** at the nonanoic acid/graphite interface**.** (b) The same STM image as in (a) but with overlaid markers showing the presence of molecules with different lengths within the monolayer. **TPTC**: blue, **QPTC**: green, **QQPTC**: red. Imaging parameters: I_{set} = 50 pA, V_{bias} = -800 mV.

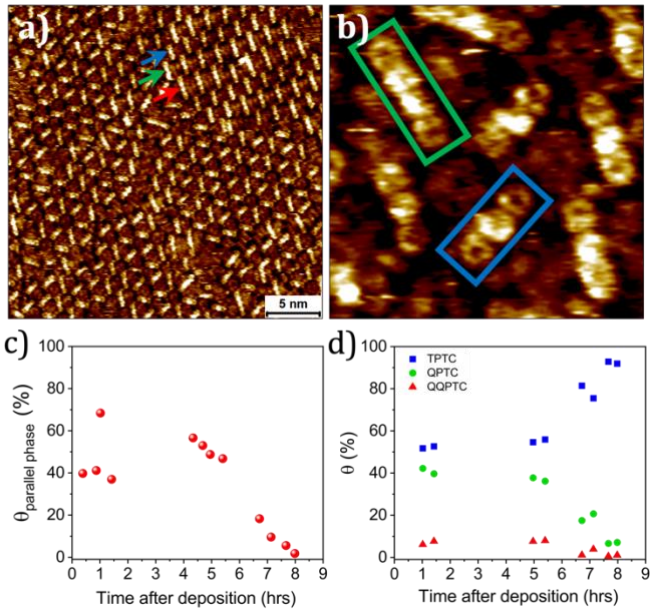

Fig. 3. (a) Representative STM image showing the presence of **QPTC** (green arrow) and **QQPTC** (red arrow) molecules in the monolayer predominantly formed by **TPTC** (blue arrow). (b) A high-resolution STM image showing co-adsorbed **QPTC** and **TPTC**. (c) Decrease in the percentage surface coverage (θ) of the parallel phase as a function of time. (d) Changes in the composition of the monolayer as a function of time. See Fig. S1 and S2 in the ESI for the calculation of the surface coverage. Imaging parameters: (a, b) I_{set} = 50 pA, V_{bias} = -800 mV.

small variation in the composition of the monolayer which changes rather abruptly afterwards. The coverage of **QPTC** decreases drastically with concomitant increase in that of **TPTC** (Fig. S6 in the ESI). The similarity in the trends observed in the disappearance of the parallel phase and the decrease of the surface coverage of **QPTC** confirms the hypothesis that the formation of the mixed parallel phase is driven by the co-adsorption of **QPTC**. As a result, the desorption of **QPTC** drives the reverse transition wherein the **TPTC** monolayer assumes the thermodynamically more stable random configuration.

The plots presented in Figure 3 point towards a two-step process where the initial desorption of the **QPTC** molecules and their replacement by **TPTC** (observed both within the parallel and the random phases) does not significantly influence the phase behavior within the first 5-6 hours. After the **QPTC/TPTC** ratio in the monolayer reaches a critical value (~0.8), the composition as well as the structure of the monolayer undergoes a drastic change. This indicates that a certain critical surface coverage of the **QPTC** is required to stabilize the parallel phase composed of **TPTC**. Once the coverage decreases below ~36%, the parallel phase is not stabilized anymore and collapses with the simultaneous increase in the coverage of the random phase, which is mostly composed of **TPTC** molecules.

To test whether annealing of the monolayer accelerates the transition from parallel to the random phase, the samples were heated at 60°C for one minute. STM imaging was carried out after the samples returned to room temperature. To our surprise, the surface still showed the presence of the parallel phase with virtually no change in the overall surface coverage of the **QPTC** molecules in the parallel phase. Furthermore, bilayer growth was observed on top of the random phase. What is peculiar is that the bilayer was found to grow exclusively on top of the random phase and was never observed atop the parallel network (Fig. 4a) (Fig. S7, S8 in the ESI). The phase-dependent growth of the bilayer indicates that the presence of the **QPTC** impurity frustrates the formation of the second layer on top of the parallel phase. Qualitatively similar results were obtained upon increasing the annealing time. The formation of a bilayer upon annealing may be related to the evaporation the of solvent causing the excess molecules present in the supernatant to adsorb onto the already formed monolayer (also see Fig. S7 ESI).

To confirm that the template layer underneath the second layer is indeed the random network, STM-based "nanoshaving"[18, 19] was carried out (Fig. S9 in the ESI). In this procedure, the second layer was "scraped" away using the STM tip by scanning at higher current setpoint (Fig. 4). It was possible to image the surface at higher tunneling currents used for removing the second layer which revealed the presence of the random network underneath as evident in Fig. 4b. Furthermore, it was also possible to follow the gradual re-growth of the second layer in the region that was subjected to nanoshaving by reverting back to lower current setpoint as depicted in Fig 4c-h (see also Fig. S10, S11 in the ESI).

The nanoshaving and the re-growth experiments described above allowed us to establish the epitaxy of the second layer with respect to the first layer, which indicates that the preferred mode of bilayer growth is such that the terphenyl backbones of the **TPTC** molecules in the top layer are adsorbed atop the H-bonded carboxyl moieties (72%). In 28% of the cases, the terphenyl backbone was found to be adsorbed atop the terphenyl unit of the molecule in the bottom layer (Fig. S12, S13 in the ESI). The preference observed here differs from that reported earlier when the bilayer growth was templated by adsorption of C_{60} in the monolayer.[15] In the latter case, no such preference was observed indicating that in the case of the guest templated bilayer, the orientation and the position of the **TPTC** molecules in the second layer are not affected by those in the bottom layer. Based on the preference observed here, it is tempting to conclude that the bottom layer dictates the adsorption of the second layer. However, simulations indicate that the adsorption energies of the **TPTC** molecules adsorbed in the top layer are similar regardless of their orientation and the position with respect to the **TPTC** molecules in the bottom layer (see Fig. S14, S15 and Table S1 in the ESI). In the absence of any energetic preference, the bilayer can thus be seen as a stack of two different **TPTC** random tiling networks driven by entropy.

The formation of the parallel phase in the monolayer, as well as the selective growth of the second layer atop the random phase after annealing, both appear to be linked to the presence of **QPTC** in the monolayer and its preference to assemble using the parallel H-bonding motif. Note that the pure **TPTC** sample always gave rise to the random tiling network under similar experimental conditions. Given that the total potential energies

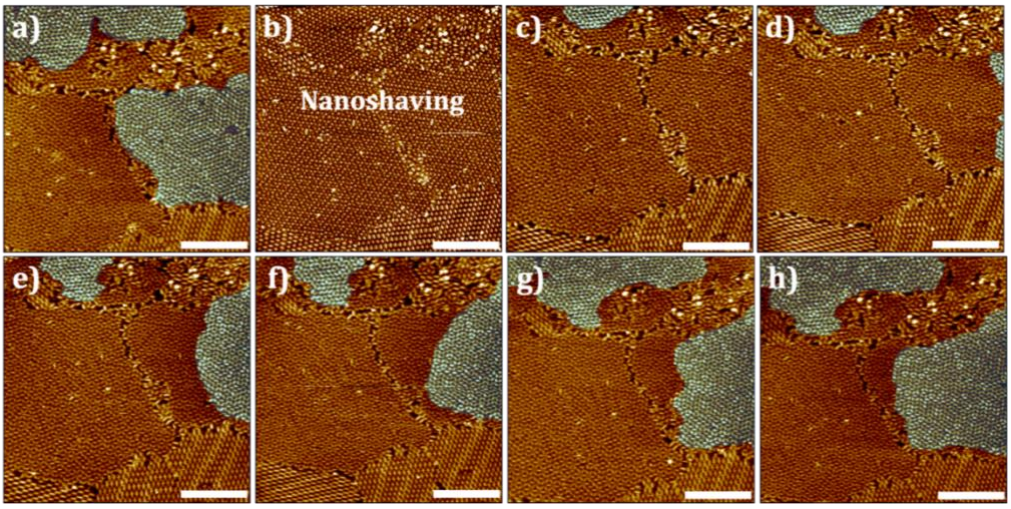

Fig. 4. A sequence of STM images showing how a second layer (highlighted in blue) formed on top of the random network (a) can be removed using nanoshaving (b) and how the slow re-growth of the domain can be followed in time using STM imaging (c-h). Scale bar = 20 nm. Imaging parameters (a, c-h): I_{set} = 50 pA, V_{bias} = -800 mV; (b) I_{set} = 300 pA, V_{bias} = -800 mV

for the hypothetical all-parallel (–123.4 kcal mol^{-1}) and the experimentally observed random tiling network (–124.06 kcal mol^{-1}) for **TPTC** are almost identical (Fig. S4 in the ESI), the preference to form the random phase appears to be driven by entropic factors. The difference in the extent of impurity in the commercial and in-house synthesized **TPTC** could arise due to different strategies used for the synthesis (see ESI for details).

In conclusion, we have demonstrated how the presence of a small percentage of an opportune impurity can change the on-surface assembly behavior *via* preferential adsorption and nucleation. The stabilization of the mixed metastable phase by the molecular dopant in the present case is kinetic in nature as evident from the slow transition to the thermodynamically stable random network. The molecular dopant not only changes the phase behavior, but it is also found to frustrate the growth of the network in the third dimension. Given the looming prospect of the incorporation of structurally similar impurities in the solid-state during synthesis, this investigation calls for a more in-depth scrutiny of the STM data not only in terms of spatial resolution but also the temporal evolution of the surface-adsorbed networks.

We thank Mr. Brent Daelemans (KUL) for his assistance with the NMR and ESI-MS characterization. The authors also gratefully acknowledge financial support from the Fund of Scientific Research Flanders (FWO), KU Leuven - Internal Funds. This work was in part supported by FWO and FNRS under EOS 30489208. The molecular modelling activities are supported by FNRS (Consortium des Équipements de Calcul Intensif – CÉCI, under Grant 2.5020.11) and by the Walloon Region (ZENOBE Tier-1 supercomputer, under grant 1117545).

Notes and references

1. A. G. Shtukenberg, S. S. Lee, B. Kahr and M. D. Ward, *Annu. Rev. Chem. Biomol. Eng.*, 2014, **5**, 77-96.
2. K. S. Mali, N. Pearce, S. De Feyter and N. R. Champness, *Chem. Soc. Rev.*, 2017, **46**, 2520-2542.
3. A. G. Slater, P. H. Beton and N. R. Champness, *Chem. Sci.*, 2011, **2**, 1440-1448.
4. U. Mazur and K. W. Hipps, *Chem. Commun.*, 2015, **51**, 4737-4749.
5. J. M. MacLeod, J. Lipton-Duffin, C. Fu, T. Taerum, D. F. Perepichka and F. Rosei, *ACS Nano*, 2017, **11**, 8901-8909.
6. L. Kampschulte, T. L. Werblowsky, R. S. K. Kishore, M. Schmittel, W. M. Heckl and M. Lackinger, *J. Am. Chem. Soc.*, 2008, **130**, 8502-8507.
7. K. V. Korpany, B. Chilukuri, K. W. Hipps and U. Mazur, *J. Phys. Chem. C*, 2020, **124**, 18639-18649.
8. X. Lu, K. W. Hipps, X. D. Wang and U. Mazur, *J. Am. Chem. Soc.*, 1996, **118**, 7197-7202.
9. J. A. A. W. Elemans, I. De Cat, H. Xu and S. De Feyter, *Chem. Soc. Rev.*, 2009, **38**, 722-736.
10. J. Teyssandier, S. D. Feyter and K. S. Mali, *Chem. Commun.*, 2016, **52**, 11465-11487.
11. K. Tahara, H. Yamaga, E. Ghijsens, K. Inukai, J. Adisoejoso, M. O. Blunt, S. De Feyter and Y. Tobe, *Nat Chem*, 2011, **3**, 714-719.
12. D. Bléger, D. Kreher, F. Mathevet, A.-J. Attias, G. Schull, A. Huard, L. Douillard, C. Fiorini-Debuischert and F. Charra, *Angew. Chem. Int. Ed.*, 2007, **46**, 7404-7407.
13. M. Blunt, X. Lin, M. d. C. Gimenez-Lopez, M. Schroder, N. R. Champness and P. H. Beton, *Chem. Commun.*, 2008, 2304-2306.
14. S. Ahn and A. J. Matzger, *J. Am. Chem. Soc.*, 2012, **134**, 3208-3214.
15. M. O. Blunt, J. C. Russell, M. d. C. Gimenez-Lopez, N. Taleb, X. Lin, M. Schröder, N. R. Champness and P. H. Beton, *Nat. Chem.*, 2011, **3**, 74-78.
16. M. O. Blunt, J. C. Russell, M. d. C. Giménez-López, J. P. Garrahan, X. Lin, M. Schröder, N. R. Champness and P. H. Beton, *Science*, 2008, **322**, 1077-1081.
17. A. Stannard, J. C. Russell, M. O. Blunt, C. Salesiotis, M. d. C. Giménez-López, N. Taleb, M. Schröder, N. R. Champness, J. P. Garrahan and P. H. Beton, *Nat. Chem.*, 2012, **4**, 112-117.
18. M. Liu, N. A. Amro and G.-y. Liu, *Annu. Rev. Phys. Chem.*, 2008, **59**, 367-386.
19. M. J. J. Coenen, T. Khoury, M. J. Crossley, B. L. M. Hendriksen, J. A. A. W. Elemans and S. Speller, *Chemphyschem*, 2014, **15**, 3484-3488.

